

# Learning to Solve Multi-Objective Routing Problems on Multigraphs

Filip Rydin<sup>1</sup>, Attila Lischka<sup>1</sup>, Jiaming Wu<sup>1</sup>, Morteza Haghiri Chehreghani<sup>2</sup>, Balázs Kulcsár<sup>1</sup>

<sup>1</sup> Chalmers University of Technology, Sweden

<sup>2</sup> Chalmers University of Technology & University of Gothenburg, Sweden  
{filipry, lischka, jiaming.wu, morteza.chehreghani, kulcsar}@chalmers.se

## Abstract

Learning-based methods for routing have gained significant attention in recent years, both in single-objective and multi-objective contexts. However, the multigraph setting, where multiple paths with distinct attributes can exist between destinations, has largely been overlooked, despite its high practical relevancy. In this paper, we introduce two neural approaches to address multi-objective routing on multigraphs. Our first approach works directly on the multigraph, by autoregressively selecting edges until a tour is completed. On the other hand, our second model first prunes the multigraph into a simple graph and then builds routes. We validate both models experimentally and find that they demonstrate strong performance across a variety of problems, including the Traveling Salesman Problem (TSP) and Capacitated Vehicle Routing Problem (CVRP)<sup>1</sup>.

## 1 Introduction

Routing problems, including the well-known Traveling Salesman Problem (TSP), are central for optimizing operations in logistics, delivery and beyond. However, these problems are generally NP-hard and difficult to solve exactly in practical, real-time settings. While exact solvers provide high-quality solutions, they do not scale well. At the same time, hand-crafted heuristics are often efficient but time-consuming to design and typically lack generalizability across problem variants.

Recently, neural solvers have emerged as a promising alternative, offering speed, accuracy, and broad applicability across routing problems (Kool, van Hoof, and Welling 2018; Ye et al. 2024; Drakulic, Michel, and Andreoli 2025). However, most learning-based approaches focus on Euclidean settings, where customers are points in a plane and travel costs are based on the Euclidean distance. Real-world road networks are far more complex and travel cost is usually asymmetric, affected by elevation, one-way streets and traffic. Further, when there are multiple conflicting criteria of importance, there can be multiple paths between customers that cannot be chosen *a priori*.

In such cases, a directed multigraph, allowing multiple, distinct paths between the same locations, is a more realistic

and powerful input-structure. In fact, using this representation has empirically been shown to increase solution quality significantly compared to the simple graph representation (Ben Ticha et al. 2017). Yet this comes at the cost of increased complexity, underscoring the need for new methods capable of handling multigraph-based routing efficiently.

The challenge intensifies in Multi-Objective (MO) routing problems, such as the Multi-Objective TSP (MOTSP), where several criteria (e.g., distance and time) must be optimized simultaneously. Even without multigraphs, MO problems are hard: not only because their single-objective counter-part is often NP-hard, but also because the number of Pareto optimal solutions can increase exponentially with the size of the problem (Ehrgott and Gandibleux 2000).

Pareto Set Learning (PSL) has recently emerged as a powerful framework for MO routing. By training offline on similar instances, PSL approximates the Pareto set quickly during inference. Moreover, since the framework is based on reinforcement learning, there is no need for oracle solvers for supervised training. These methods have shown strong results in Euclidean settings (Lin, Yang, and Zhang 2022; Fan et al. 2025), but there is currently no general PSL framework for routing on multigraphs or in non-Euclidean settings, despite their higher practical relevance.

We attempt to bridge this gap. Concretely, our main contributions are:

- We extend PSL to handle multigraph inputs, where the model selects not only the next node but also the path taken. To our knowledge, this is the first neural solver designed for such input structures. Although we treat multi-objective optimization, we hypothesize that our approach can be useful in single-objective constrained and stochastic cases too.
- As a byproduct, our model constitutes the first general-purpose, multi-objective solver capable of handling a variety of routing problems on asymmetric graphs.
- In order to do this, we propose two separate models: One edge-based that is simple and accurate but relatively slow and one dual-task model that first sparsifies the multigraph into a simple graph and then selects routes. The latter is faster but more complex.
- Experimentally, we show that our approach achieves competitive results for several MO routing problems

<sup>1</sup>Our code will be made publicly available upon acceptance of the paper.

on asymmetric graphs and multigraphs, including the MOTSP, Multi-Objective Capacitated Vehicle Routing Problem (MOCVRP) and MOTSP with time-windows.

## 2 Related Work

### 2.1 Learning for Routing

Motivated by the success of end-to-end learning rather than hand-crafted heuristics in fields such as image classification and language modeling, neural heuristics for routing have gained increasing attention during the last years. Broadly, methods can be classified by how they obtain the tours. Two prominent alternatives are *autoregressive construction*, based on iterative building of tours one node at a time, and *non-autoregressive construction*, that outputs heatmaps in a one-shot fashion for down-stream decoding with some search method.

Early works in the first category include Vinyals, Fortunato, and Jaitly (2015), which utilized an oracle TSP solver for supervised learning, and Bello et al. (2017), which introduced reinforcement learning for training. By using attention models and inherent symmetries in the problem, first Kool, van Hoof, and Welling (2018) and then Kwon et al. (2020) obtained close to 0 optimality gap on various routing problems. Regarding asymmetric problems, Kwon et al. (2021) proposed MatNet, a mixed-attention architecture working on bi-partite graphs. More recent works are Jin et al. (2023); Drakulic et al. (2023); Chen et al. (2024); Bi et al. (2024). These papers have improved results, can handle constraints better and can scale to even larger problems than previously. Another notable example is Drakulic, Michel, and Andreoli (2025), where one model learns to solve a multitude of combinatorial optimization problems, including examples from routing.

In the second category, some notable works are Joshi, Laurent, and Bresson (2019); Fu, Qiu, and Zha (2021); Qiu, Sun, and Yang (2022); Sun and Yang (2023). Typically, these methods perform worse than autoregressive approaches, but scale better to large instances due to lower space and time complexity. An interesting recent work combining the two approaches to solve large instances (up to  $10^5$  nodes for the TSP) is Ye et al. (2024).

### 2.2 Multi-Objective Learning for Routing

The literature on multi-objective routing is more sparse than in the single-objective case. Some early works (Li, Zhang, and Wang 2021; Wu, Wang, and Zhang 2020) utilize multiple models, where one model is responsible for one preference between the objectives. This quickly becomes infeasible as the number of models required grows exponentially with the number of objectives (Ehrgott 2005). Pareto-set learning for multi-objective routing using a single model was proposed in Lin, Yang, and Zhang (2022). They used the hyper-networks of Navon et al. (2021) to condition the decoder on the preference. Recent papers that feature improved results with a similar conditioning method include Fan et al. (2025); Lu et al. (2024). An alternative approach is to use meta-learning to train a single model that can be quickly fine-tuned over a few steps to solve individual subproblems.

Two representative works in this direction are Zhang et al. (2021); Chen et al. (2023a).

Regarding asymmetric problems in the context of multi-objective optimization, the only existing learning-based methods we are aware of are those proposed in Santiyuda et al. (2024) and Zhou, Kong, and Wang (2025). Notably, both of these methods are tailored to particular problem types and evaluated within narrowly defined domains. In contrast, our approach is designed with a very general framework, capable of handling a broad class of routing problems.

### 2.3 Routing on Multigraphs

In the multi-objective case, a multigraph is often a more suitable representation of a road network than a simple graph. In fact, this network model has become more and more common for MO shortest path problems. One solution is genetic algorithms, see for instance Beke, Weiszer, and Chen (2021) for a comprehensive benchmarking study. Other studies have proposed A\*-related algorithms, e.g., AMOA\* (Weiszer, Burke, and Chen 2020) and MOMGA\* (Liu, Chen, and Weiszer 2022), to efficiently obtain a Pareto set of shortest paths.

The multigraph framework has also been applied to routing problems, but to a lower extent. The first study in this regard was Garaix et al. (2010), who designed a simple heuristic and branch-and-price method for a single-objective on-demand transportation problem. Other works proposing either exact solvers or heuristics for single-objective constrained problems or multi-objective problems are Lai, Caliskan Demirag, and Leung (2016); Ben Ticha et al. (2019); Tikani, Setak, and Demir (2021). In addition, a particularly interesting study is Ben Ticha et al. (2017), where it is clearly concluded that a multigraph setup yields significantly lower costs compared to a simple graph representation for the capacitated vehicle routing problem with time-windows. On real-world instances, a solution cost reduction of up to 10.5% is reported. At the same time, the computation time increases significantly under this perspective, and the authors highlight the need for new heuristics.

We believe learning-based methods can fill this niche, as they have proven to be efficient, effective and broadly applicable. To the best of our knowledge, this work presents the first learning-based routing approach to address problems on multigraphs.

## 3 Multi-Objective Optimization

A general multi-objective optimization problem can be written as

$$\min_{x \in X} f(x),$$

where  $f : X \rightarrow \mathbb{R}^m$  and  $m > 1$ . Unlike the Single-Objective (SO) case, the solution to such a problem is not one objective value with corresponding optimal solutions but a set of values known as the Pareto Front (PF) with corresponding solutions in the Pareto Set (PS). Formally, we define the PS as the set

$$\text{PS} := \{x \in X \mid \nexists x' \in X : f(x') \prec f(x)\},$$

where  $f(x') \prec f(x)$  denotes that  $f(x')$  dominates  $f(x)$ , meaning

$$\begin{aligned} f_i(x') &\leq f_i(x) \quad \forall i = 1, \dots, m, \\ f_j(x') &< f_j(x) \text{ for at least one } j. \end{aligned}$$

Correspondingly, the Pareto Front (PF) is defined as the image of the Pareto Set under  $f$ , that is,

$$\text{PF} := \{f(x) \in \mathbb{R}^m \mid x \in \text{PS}\}.$$

Intuitively, the PS represents solutions for which no strictly better alternative exists.

To obtain this set, a typical method is decomposition through scalarization. The idea is to translate the MO problem into several SO problems that can be solved in parallel or consecutively. Let  $\lambda \in \mathbb{R}^m$  such that  $\lambda_i \geq 0 \forall i$  and  $\sum_i \lambda_i = 1$  be a vector that controls the preference among the objectives. Then, the most straight-forward scalarization is the *Linear Scalarization* (LS)  $f_\lambda(x) = \sum_i \lambda_i f_i(x)$ . The LS subproblem is then  $\min_x f_\lambda(x)$ , which is a standard SO problem. Unfortunately, it is well-known that there may be solutions in the Pareto Set that do not solve an LS subproblem for any preference  $\lambda$  (Ehrgott 2005). The *Chebyshev Scalarization* has more favorable properties. Let  $z_i^*$  be an ideal value for objective  $i$ . Then the Chebyshev scalarized cost is

$$f_\lambda(x) = \max_i \{\lambda_i |f_i(x) - z_i^*|\}. \quad (1)$$

Given a solution in the PS, there always exists a preference  $\lambda$  and corresponding subproblem for which the solution is optimal (Choo and Atkins 1983).

In our context of multigraphs, it is interesting to consider how the problem simplifies under scalarization. We note that under LS, the MOTSP on a multigraph can be simplified to a simple graph by pruning edges that have sub-optimal LS cost compared to a parallel edge. Under Chebyshev scalarization or for more complicated problems this simple method will not work. Instead, we propose to learn which parallel edge is optimal while simultaneously learning to construct the optimal route.

## 4 GNN-Based Multigraph Solver

In the following, we detail two approaches based on Graph Neural Networks (GNNs) for solving MO multigraph routing problems. We call our method GNN-based Multigraph Solver (GMS) and propose an edge-based variant, which is slow but simple, as well as an architecture with two decoders, which is faster but more complex. Both of these utilize the Graph Edge Attention Network (GREAT) of Lischka et al. (2024) as the encoder, the reason being that it 1) Can handle input data structured as multigraphs; 2) Outputs edge-embeddings; 3) Has been applied in an autoregressive-framework and shown competitive performance for non-Euclidean SO problems. However, note that it is possible to use other architectures in the encoder, such as e.g., the anisotropic GNN of Sun and Yang (2023).

Specifically, we utilize the Node-Based (NB) version of GREAT. We refer the reader to Lischka et al. (2024) for details. Here, it suffices to say that the core component of an

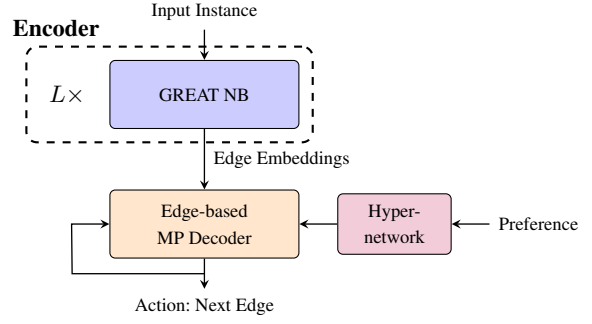


Figure 1: Edge-Based GMS

NB GREAT-layer is an attention sublayer, that utilizes attention scores  $\alpha'$  and  $\alpha''$  to compute a temporary node-feature  $x$  for each node  $i$  according to

$$x_i = \left( \sum_{l \in E^+(i)} \alpha'_{il} W'_1 e_l \parallel \sum_{l' \in E^-(i)} \alpha''_{il'} W''_1 e_{l'} \right).$$

Here,  $\parallel$  is the concatenation operation,  $e_l$  denotes an edge embedding for edge  $l$ ,  $W'_1$  and  $W''_1$  are trainable weight matrices and  $E^+(i)$ ,  $E^-(i)$  denote outgoing and incoming edges respectively. New edge embeddings are then computed according to

$$e'_l = W_2 (x_{\text{start}(l)} \parallel x_{\text{end}(l)}), \quad (2)$$

where  $\text{start}(l)$  and  $\text{end}(l)$  denote the start and end nodes of the directed edge  $l$ . The attention layers are arranged into a single GREAT-layer together with feed-forward layers, residual connections and normalization according to the original transformer architecture (Vaswani et al. 2017). Note that the residual connections are important as they allow parallel edges to have differing embeddings.

### 4.1 Edge-Based GMS

We visualize Edge-Based GMS (GMS-EB) in Figure 1. The encoder, consisting of  $L$  GREAT-layers, outputs edge embeddings. Using these, the decoder constructs valid tours auto-regressively. As in Lin, Yang, and Zhang (2022); Navon et al. (2021) we utilize a hyper-network to generate the weights of the decoder conditioned on the current preference. The decoder is an edge-based variant of the Multi-Pointer (MP) decoder from Jin et al. (2023), which we detail in Appendix A. Given the context of the current node in the tour, the decoder outputs probabilities of traversing edges starting in that node.

Note that the underlying graphs in routing problems are usually complete. Hence there are  $N^2$  edges in a graph of  $N$  nodes. Moreover, the decoder needs to be run  $N$  times to construct a full tour and we usually roll out  $N$  sample trajectories. Hence an edge-based decoder scales according to  $N^4$  compared to a node-based that scales according to  $N^3$ . We find that this is a bottleneck in terms of memory requirements and inference time. Hence we propose a second architecture that utilizes a node-based decoder.

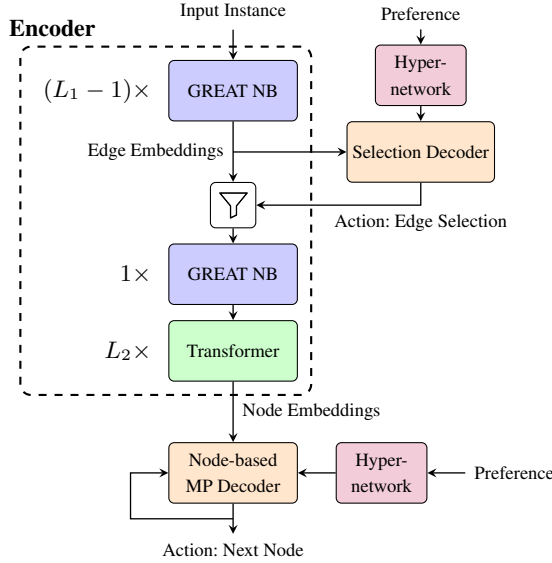


Figure 2: Dual Head GMS

## 4.2 Dual Head GMS

Using GREAT, we can obtain node-embeddings by not applying (2) in the final layer. The problem is that the action of selecting a node is not sufficient, as a path selection is also needed. Thus, we need to ensure that the action of choosing a node uniquely defines which edge to choose, which is achieved by pruning parallel edges leaving a unique one between each node-pair. In general, choosing this edge is not trivial. Thus, we propose to learn the choice using a dual decoder setup.

We call this approach Dual Head GMS (GMS-DH) and it is visualized in Figure 2. The key is that we insert a second decoder before the final encoder layer. This decoder uses the intermediate edge-embeddings to select which parallel edge to keep. The selection is fed back into the encoder, which only propagates the embedding of the remaining edges and converts them to node-embeddings. We also find it beneficial to add a small number of standard transformer layers after the final GREAT-layer in order to obtain more expressive node-embeddings. We detail the architecture for the selection-decoder in Appendix A. For the routing-decoder, we use a preference-conditioned version of the Multi-pointer decoder (Jin et al. 2023). When applying GMS-DH to simple graphs, we simply remove the first decoder. Also note that this architecture ensures that the first  $L_1 - 1$  layers only need to be run once for each instance, which reduces the run-time compared to selecting edges before encoding.

From a broader perspective, our approach in GMS-DH can be viewed as a mixture of non-autoregressive and autoregressive learning. As a drawback, the edge-choice can no longer depend on the routing context, instead it must be chosen before the roll-out is started.

## 4.3 Training Algorithm

Our first proposed model, GMS-EB, is trained using the Multi-Objective REINFORCE from Lin, Yang, and Zhang (2022). In short, given a preference  $\lambda \sim \Lambda$  and instance  $s \sim S$ , the model parameterizes a policy  $p_{\theta(\lambda)}(\cdot | s)$ . A tour  $\pi$  is associated with a reward according to (1)

$$R_{\lambda}(\pi) = -\max_i \{\lambda_i | f_i(\pi) - z_i^* | \}. \quad (3)$$

The objective is to maximize

$$J(\theta) = \mathbb{E}_{\pi \sim p_{\theta}, \lambda \sim \Lambda, s \sim S} [R_{\lambda}(\pi)].$$

Additionally, we form a baseline  $b_{\lambda}(s_i)$  by rolling out  $K$  tours for the same instance  $s_i$  and averaging the reward, according to the POMO framework (Kwon et al. 2020), to stabilize the training. The policy gradient is utilized to update the model weights and it is approximated, given one preference  $\lambda$ , according to

$$\nabla J(\theta) \approx \frac{1}{BK} \sum_{i,j=1}^{B,K} A_{ij} \nabla_{\theta} \log(p_{\theta(\lambda)}(\pi_{ij} | s_i)),$$

where  $B$  is the batch size of instances and the advantage is

$$A_{ij} = R_{\lambda}(\pi_{ij}) - b_{\lambda}(s_i).$$

For the second model, the training is more complicated. We can view each head as an agent. The selection-head takes actions corresponding to which edge to choose between each node pair. It parameterizes a policy  $q_{\tilde{\theta}(\lambda)}(\cdot | s)$ . The routing-head uses the selection, which we denote by  $e \sim q_{\tilde{\theta}(\lambda)}$ . It parameterizes a policy  $p_{\theta(\lambda)}(\cdot | s, e)$  and obtains a scalar reward  $R_{\lambda}^{(2)}(\pi) = R_{\lambda}(\pi)$  according to (3). With a fixed  $\tilde{\theta}$ , the objective for this head is to maximize

$$J_2(\theta) = \mathbb{E}_{\pi \sim p_{\theta}, \lambda \sim \Lambda, s \sim S, e \sim q_{\tilde{\theta}}} [R_{\lambda}^{(2)}(\pi)].$$

On the other hand, the task of the selection-head is to ensure that the edge selection is optimal. Let  $\tilde{\pi}(e)$  denote the optimal tour given edge selection  $e$ . Then, define

$$R_{\lambda}^{(1)}(e) = R_{\lambda}(\tilde{\pi}(e)),$$

$$J_1(\tilde{\theta}) = \mathbb{E}_{\lambda \sim \Lambda, s \sim S, e \sim q_{\tilde{\theta}}} [R_{\lambda}^{(1)}(e)].$$

As the optimal tour  $\tilde{\pi}$  is not available, we approximate it using  $K_2$  sampled tours  $\pi_1, \dots, \pi_{K_2} \sim p_{\theta(\lambda)}(\cdot | s, e)$ :

$$R_{\lambda}^{(1)}(e) \approx \max_{k=1, \dots, K_2} R_{\lambda}(\pi_k). \quad (4)$$

A baseline  $b_{\lambda}^{(1)}(s_i)$  for the selection-head is formed by averaging  $R^{(1)}$  over  $K_1$  samples while a baseline  $b_{\lambda}^{(2)}(s_i, e_{ij})$  for the routing-head is formed by averaging over the  $K_2$  samples for a fixed  $s_i$  and  $e_{ij}$ . Thus, we approximate the policy

---

**Algorithm 1: One batch of REINFORCE for GMS-DH**

---

**Input:** Preference distribution  $\Lambda$ , instance distribution  $S$ , batch size  $B$ , number of samples per instance head 1,  $K_1$ , and head 2,  $K_2$

- 1: Sample preference  $\lambda \sim \Lambda$
  - 2: Sample instances  $s_i \sim S, i = 1, \dots, B$
  - 3: Select edges  $e_{ij} \sim q_{\tilde{\theta}(\lambda)}(\cdot | s_i), j = 1, \dots, K_1$
  - 4: Sample tours  $\pi_{ijk} \sim p_{\theta(\lambda)}(\cdot | s_i, e_{ij}), k = 1, \dots, K_2$
  - 5: Calculate  $R_\lambda^{(1)}(e_{ij}), R_\lambda^{(2)}(\pi_{ijk}), b_\lambda^{(1)}(s_i)$  and  $b_\lambda^{(2)}(s_i, e_{ij})$
  - 6: Calculate gradients  $\nabla J_1(\tilde{\theta}), \nabla J_2(\theta)$  with (5)
  - 7:  $\tilde{\theta} \leftarrow \mathbf{ADAM}(\tilde{\theta}, \nabla J_1(\tilde{\theta})), \theta \leftarrow \mathbf{ADAM}(\theta, \nabla J_2(\theta))$ ,
- 

gradients with

$$\begin{aligned} \nabla J_1(\tilde{\theta}) &\approx \frac{1}{BK_1} \sum_{i,j=1}^{B,K_1} A_{ij}^{(1)} \nabla_{\tilde{\theta}} \log(q_{\tilde{\theta}}(e_{ij} | s_i)), \\ \nabla J_2(\theta) &\approx \frac{1}{BK_1K_2} \sum_{i,j,k=1}^{B,K_1,K_2} A_{ijk}^{(2)} \nabla_{\theta} \log(p_{\theta}(\pi_{ijk} | s_i, e_{ij})), \\ A_{ij}^{(1)} &= R_\lambda^{(1)}(e_{ij}) - b_\lambda^{(1)}(s_i), \\ A_{ijk}^{(2)} &= R_\lambda^{(2)}(\pi_{ijk}) - b_\lambda^{(2)}(s_i, e_{ij}). \end{aligned} \quad (5)$$

For easy reference, we outline the training of GMS-DH in Algorithm 1.

In addition, for both models we utilize a curriculum learning approach to speed up training. We start by training on small graph sizes and then gradually increase the problem size. For GMS-DH in the multigraph setting, we also start by training the routing-head on simple graphs to ensure that the approximation (4) is accurate even during the initial epochs of multigraph training. Further details regarding the curriculum learning can be found in Appendix B.

## 5 Experimental Studies

In this section we show the empirical performance for our two proposed methods on several routing problems across multiple instance sizes and distributions. We compare against evolutionary algorithms, neural baselines and state-of-the-art single-objective heuristics.

### 5.1 Benchmarking Setup

**Problems:** In the asymmetric simple graph case we consider two standard routing problems: The Multi-Objective Traveling Salesman Problem (MOTSP) and Multi-Objective Capacitated Vehicle Routing Problem (MOCVRP). Specifically, we consider bi-objective variants of these. In the MOTSP, we sample two distances for each node pair. These are summarized over the tour to yield the objective values. Regarding the distances, we consider both the TMAT (Kwon et al. 2021) and XASY distributions (Gaile et al. 2022),

where the former obeys the triangle inequality and the latter does not - making it more difficult. For the MOCVRP, we sample one distance according to these distributions. We then let the first objective be given by the total distance of a tour and the second objective by the makespan, which is the longest trip for a single vehicle. This is a standard benchmark problem in literature (Lin, Yang, and Zhang 2022).

In the multigraph setting, we consider the Multigraph MOTSP (MGMOTSP) with two objectives, where we sample two-dimensional edge distances using distributions called FIX $x$  and FLEX $x$ . Here,  $x$  denotes the number of edges between each node pair. In the FLEX-distribution, we sample edge distances independently and remove edges which are dominated. In the FIX distribution we first sample edges independently, but then rearrange by sorting, so that the an edge that is best in one objective is the worst in the other objective and so on. Thus, in the FIX $x$ -distribution there are always exactly  $x$  edges between each node pair, whereas FLEX $x$  has at most  $x$  edges.

In Appendix C, we provide more in-depth explanations of the problems and distributions. We also provide results on Euclidean problems in Appendix E.

**Baselines:** For the MOTSP and MGMOTSP, we utilize linear scalarization together with strong single-objective methods in the form of LKH3 (Helsgaun 2017) and Google OR-tools. We also benchmark against four Multi-Objective Evolutionary Algorithms (MOEAs): MOGLS (Ishibuchi and Murata 1998), MOEA/D (Zhang and Li 2007), NSGA-II (Deb et al. 2002) and NSGA-III (Blank, Deb, and Roy 2019). Below, we only show the results for the MOEA that performs best in each scenario. Finally, we design a neural baseline using the MatNet-architecture (Kwon et al. 2021) as encoder and a preference-conditioned MP network as decoder. We call this MatNet-Based Model (MBM) and our motivation is that this is a learning-based method that can be used almost "off-the-shelf" by combining components from literature. In the multigraph setting, this architecture requires us to pre-process the input by pruning edges until we obtain a simple graph, which we do using linear scalarization.

In Appendix A and D, we provide further details about the neural benchmark and MOEAs respectively. In Appendix E, we also show results for all MOEAs as well as some other weaker heuristics.

**Model Settings:** We train all models for 200 epochs using 100 000 randomly generated instances per epoch with the ADAM optimizer (Kingma and Ba 2015) and a learning-rate of  $\eta = 10^{-4}$ . For GMS-EB we let the number of layers be  $L = 6$ , while GMS-DH has  $L_1 = 5$  and  $L_2 = 2$ . For both models we use 128 as the embedding dimension and 8 attention heads in the GREAT layers and MP decoders. Regarding the number of samples in the decoding, we set  $K_1 = 4$  for the selection-decoder during training and  $K_1 = 1$  during inference. In the routing-decoder, we always set  $K_2$  to the problem size as customary in the POMO framework (Kwon et al. 2020). Finally, we augment the models during inference with a factor of 8. For MBM, this is done using the original MatNet-augmentation (Kwon et al. 2021), while for GMS we use the scaling-augmentation of Lischka et al. (2024).

		TMAT50			TMAT100			XASY50			XASY100		
		HV	Gap	Time									
MOTSP	LKH	0.58	0.00%	(6.4m)	0.63	0.00%	(29m)	0.83	0.00%	(6.9m)	0.90	0.00%	(32m)
	OR Tools	0.54	6.13%	(29m)	0.59	7.12%	(2.5h)	0.77	7.25%	(24m)	0.85	6.06%	(1.8h)
	MOEA/D	0.53	9.51%	(3.7h)	0.50	20.9%	(13h)	0.73	12.68%	(3.6h)	0.70	22.22%	(13h)
	MBM	0.50	13.5%	(3.9s)	0.56	11.2%	(19s)	0.75	10.37%	(3.7s)	0.84	7.41%	(19s)
	MBM (aug)	0.52	10.2%	(27s)	0.58	9.17%	(2.4m)	0.76	8.28%	(27s)	0.85	6.34%	(2.4m)
	GMS-EB	0.57	1.50%	(25s)	0.63	1.45%	(3.6m)	0.81	2.94%	(25s)	0.88	3.03%	(3.6m)
	GMS-DH	0.57	2.36%	(4.1s)	0.62	2.76%	(20s)	0.80	4.12%	(3.9s)	0.86	4.87%	(20s)
	GMS-EB (aug)	<b>0.57</b>	<b>1.14%</b>	(3.3m)	<b>0.63</b>	<b>1.13%</b>	(29m)	<b>0.82</b>	<b>2.06%</b>	(3.3m)	<b>0.88</b>	<b>2.76%</b>	(28m)
	GMS-DH (aug)	0.57	1.76%	(28s)	0.62	2.19%	(2.6m)	0.81	2.84%	(28s)	0.87	3.85%	(2.6m)
			TMAT50			TMAT100			XASY50			XASY100	
MOCVRP	MOEA/D	0.41	13.98%	(24h)	0.19	58.70%	(76h)	0.65	13.88%	(24h)	0.42	47.23%	(83h)
	MBM	0.47	1.33%	(6.2s)	0.43	4.50%	(27s)	0.70	6.57%	(6.2s)	0.60	24.47%	(27s)
	MBM (aug)	0.47	0.99%	(41s)	0.44	3.29%	(3.3m)	0.72	4.13%	(42s)	0.64	19.60%	(3.4m)
	GMS-EB	0.47	0.25%	(36s)	0.45	0.57%	(4.2m)	0.74	1.89%	(36s)	0.79	1.23%	(4.3m)
	GMS-DH	0.47	0.76%	(6.8s)	0.45	1.46%	(32s)	0.72	4.13%	(6.6s)	0.77	3.60%	(33s)
	GMS-EB (aug)	<b>0.47</b>	<b>0.00%</b>	(5.0m)	<b>0.45</b>	<b>0.00%</b>	(33m)	<b>0.75</b>	<b>0.00%</b>	(4.9m)	<b>0.80</b>	<b>0.00%</b>	(48m)
	GMS-DH (aug)	0.47	0.36%	(47s)	0.45	0.79%	(4.3m)	0.74	1.65%	(47s)	0.79	1.21%	(4.7m)
		FLEX2-50			FLEX2-100			FIX2-50			FIX2-100		
MGMOTSP	LKH	0.90	0.00%	(6.3m)	0.94	0.00%	(31m)	0.92	0.00%	(6.3m)	0.95	0.00%	(30m)
	OR Tools	0.86	4.21%	(24m)	0.91	3.46%	(1.8h)	0.90	2.59%	(24m)	0.93	2.25%	(2.0h)
	MOEA/D	0.74	17.50%	(18h)	0.66	30.28%	(12h)	0.78	15.42%	(18h)	0.69	27.63%	(12h)
	MBM	0.86	5.21%	(13s)	0.91	3.72%	(44s)	0.90	2.46%	(13s)	0.93	2.41%	(44s)
	MBM (aug)	0.87	3.98%	(1.7m)	0.91	3.28%	(5.9m)	0.91	1.66%	(1.7m)	0.93	2.10%	(5.9m)
	GMS-EB	0.88	2.00%	(56s)	0.93	1.81%	(9.1m)	0.91	1.27%	(57s)	0.94	1.33%	(9.2m)
	GMS-DH	0.89	1.84%	(13s)	0.92	2.11%	(49s)	0.91	1.73%	(12s)	0.93	2.13%	(52s)
	GMS-EB (aug)	0.89	1.50%	(7.5m)	<b>0.93</b>	<b>1.47%</b>	(1.2h)	<b>0.91</b>	<b>1.02%</b>	(7.5m)	<b>0.94</b>	<b>1.09%</b>	(1.2h)
	GMS-DH (aug)	<b>0.89</b>	<b>1.45%</b>	(1.5m)	0.93	1.61%	(6.6m)	0.91	1.40%	(1.5m)	0.93	1.92%	(6.6m)

Table 1: MOTSP, MOCVRP and MGMOTSP with different instance sizes (50, 100) and distributions. Runtime is for solving 200 instances.

**Metrics:** We utilize the Hypervolume (HV) metric (Zitzler et al. 2003) to evaluate the performance of the methods. Formally, for a given set of points  $S = \{y_1, \dots, y_n\} \subset \mathbb{R}^m$  and a reference point  $r \in \mathbb{R}^m$  that is dominated by all points in  $S$ , the HV is defined as:

$$\text{HV}(S, r) = \lambda \left( \bigcup_{i=1}^n [y_i, r] \right),$$

where  $\lambda$  denotes the Lebesgue measure in  $\mathbb{R}^m$ , and  $[y_i, r]$  represents the axis-aligned hyperrectangle bounded by  $y_i$  and  $r$ . Intuitively, a higher HV generally indicates better performance.

In our experiments, we report the normalized HV, which is scaled to lie in the interval  $[0, 1]$ , averaged over 200 test instances. For the neural models we use 101 preferences during inference, which is also the number of subproblems for the benchmarks relying on scalarization. Apart from the HV, we provide the HV gap compared to the best-performing method as well as the inference time. In Appendix B, we

also report some training times for the learning-based methods. For these methods, we used one NVIDIA Tesla A40 GPU with 48GB VRAM during training and inference. The non-learning-based methods were all tested using an Intel Xeon Gold 6338 CPU and 8 parallel processes.

## 5.2 Performance on Benchmark Problems

We show the performance of GMS together with the benchmarks in Table 1. As can be seen, GMS outperforms all benchmarks except LKH on the MOTSP and MGMOTSP, while it is the best performing model on the MOCVRP. This showcases that our architectures are generally applicable across a variety of distributions, instance sizes and problems. We note that the runtime for GMS-EB scales poorly with the problem size, but it is still fast compared to most benchmarks, especially without augmentation.

	FLEX2-20			FLEX2-50		
	HV	Gap	Time	HV	Gap	Time
MOEA/D	0.75	9.19%	(2.7h)	0.60	32.79%	(34h)
MBM	0.72	12.89%	(4.9s)	0.80	11.09%	(14s)
MBM (aug)	0.73	11.98%	(34s)	0.81	10.10%	(1.8m)
GMS-EB	0.81	1.95%	(4.3s)	0.89	0.97%	(60s)
GMS-DH	0.80	3.37%	(3.1s)	0.85	5.10%	(13s)
GMS-EB (aug)	0.82	0.00%	(31s)	0.90	0.00%	(7.9m)
GMS-DH (aug)	0.82	0.33%	(16s)	0.87	2.69%	(1.6m)

Table 2: MGMOTSPTW with different node counts. Again, runtime is for 200 instances.

### 5.3 Multigraph Problem without Clear Pruning

The main motivation behind learning to select edges in the multigraphs is to plan routes when no clear pruning method exists. Thus, we evaluate the performance on such a problem as well. Specifically, we consider an MGMOTSP with Time-Windows (MGMOTSPTW). Each edge is associated with a time and distance, while the objectives correspond to the number of violated time-windows and the total distance. Unlike the MGMOTSP with linear scalarization, it is not clear in this case which edges can be pruned a priori due to the more intricate time-window objective.

We display the performance on this problem in Table 2, and benchmark against MBM with LS pruning as well as MOEAs. Evidently, our models are the best performing ones, illustrating the value of learning to select edges in combination with learning-to-route.

### 5.4 Zero-Shot Generalization

We also test our models in a zero-shot setting on larger instances, which is displayed in Table 3. Both GMS-DH and GMS-EB remain competitive across both problems and all distributions.

	TMAT200			XASY200			
	HV	Gap	Time	HV	Gap	Time	
MOTSP	LKH	0.67	0.00%	(1.2h)	0.95	0.00%	(1.3h)
	OR Tools	0.62	7.89%	(6.5h)	0.90	4.46%	(4.0h)
	GMS-EB	<b>0.66</b>	<b>1.86%</b>	(17m)	<b>0.92</b>	<b>2.78%</b>	(17m)
	GMS-DH	0.65	3.59%	(1.0m)	0.90	5.22%	(1.0m)
	FLEX2-200			FIX2-200			
	HV	Gap	Time	HV	Gap	Time	
MGMOTSP	LKH	0.97	0.00%	(1.2h)	0.97	0.00%	(1.2h)
	OR Tools	0.94	2.53%	(3.9h)	0.95	1.73%	(4.0h)
	GMS-EB	<b>0.95</b>	<b>1.74%</b>	(50m)	<b>0.96</b>	<b>1.34%</b>	(50m)
	GMS-DH	0.95	2.27%	(2.2m)	0.94	2.56%	(2.2m)

Table 3: MOTSP and MGMOTSP for larger instances (zero-shot generalization). Performance over 100 instances.

### 5.5 Ablation Study

Finally, we showcase the ability of the selection-decoder in GMS-DH to select beneficial edges. Table 4 shows the result

	FLEX2-50	
	HV	Gap
GMS-DH (Ch. Reward)	<b>0.8862</b>	<b>1.84%</b>
GMS-DH (Lin. Reward)	0.8781	2.74%
GMS-DH Simple (Lin. Reward)	0.8789	2.65%
GMS-DH Simple (Ch. Reward)	0.8847	2.00%

Table 4: Ablation of the selection-decoder in GMS-DH by replacing it with a simple pruning function. Results are for the MGMOTSP.

when replacing this component with a simple pruning function that removes edges with suboptimal linearly scalarized cost. For fairness, we also benchmark using both linearly scalarized reward and Chebyshev reward. As discussed, in the linear case the pruning should be optimal.

Evidently, Chebyshev reward improves the results substantially. Moreover, learning the selection compared to using a simple function also seems slightly better, even in the simple case of the MGMOTSP.

## 6 Conclusion and Future Work

In this paper, we propose two methods to learn to construct solutions for routing problems on multigraphs. We highlight that while we solve problems with multiple objectives, our models can be valuable in all scenarios with no clear choice between alternative paths. In future works, we will apply our methods on more advanced problems.

A key weakness of our approach is that GMS-DH does not quite reach the same performance as GMS-EB in most cases. In this regard, there are works that are tangential to ours that could be utilized to obtain even better results for either GMS-DH or GMS-EB. Examples include the HV training of Lu et al. (2024) and diversity enhancement of Chen et al. (2023b). In the future, we will also explore decomposition methods like Ye et al. (2024) to extend our approach to even larger problem sizes.

Finally, from a broader perspective, we want to stress that routing problems on multigraphs are not well explored in literature. We believe one major reason is because of the complexity this formulation introduces. Learning-based methods can help alleviate this weakness and make the multigraph formulation more appealing.

## Acknowledgements

This work was performed as a part of the research project ‘‘LEAR: Robust LEARNING methods for electric vehicle Route selection’’ funded by the Swedish Electromobility Centre (SEC). The computations were enabled by resources provided by the National Academic Infrastructure for Supercomputing in Sweden (NAISS) at Chalmers e-Commons partially funded by the Swedish Research Council through grant agreement no. 2022-06725. Through the affiliation of F.R., the work was also partially supported by the Wallenberg AI, Autonomous Systems and Software Program (WASP) funded by the Knut and Alice Wallenberg Foundation.

## References

- Beke, L.; Weiszter, M.; and Chen, J. 2021. A Comparison of Genetic Representations and Initialisation Methods for the Multi-objective Shortest Path Problem on Multigraphs. *SN Computer Science*, 2(3): 176.
- Bello, I.; Pham, H.; Le, Q. V.; Norouzi, M.; and Bengio, S. 2017. Neural Combinatorial Optimization with Reinforcement Learning. In *International Conference on Learning Representations*, volume 5.
- Ben Ticha, H.; Absi, N.; Feillet, D.; and Quilliot, A. 2017. Empirical Analysis for the VRPTW with a Multigraph Representation for the Road Network. *Computers & Operations Research*, 88: 103–116.
- Ben Ticha, H.; Absi, N.; Feillet, D.; and Quilliot, A. A. 2019. Multigraph Modeling and Adaptive Large Neighborhood Search for the Vehicle Routing Problem with Time Windows. *Computers and Operations Research*, 104: 113–126.
- Bi, J.; Ma, Y.; Zhou, J.; Song, W.; Cao, Z.; Wu, Y.; and Zhang, J. 2024. Learning to Handle Complex Constraints for Vehicle Routing Problems. In *Advances in Neural Information Processing Systems*, volume 37.
- Blank, J.; Deb, K.; and Roy, P. C. 2019. Investigating the Normalization Procedure of NSGA-III. In *Evolutionary Multi-Criterion Optimization*, 229–240.
- Chen, J.; Gong, Z.; Liu, M.; Wang, J.; Yu, Y.; and Zhang, W. 2024. Looking Ahead to Avoid Being Late: Solving Hard-Constrained Traveling Salesman Problem. ArXiv:2403.05318.
- Chen, J.; Wang, J.; Zhang, Z.; Cao, Z.; Ye, T.; and Chen, S. 2023a. Efficient Meta Neural Heuristic for Multi-Objective Combinatorial Optimization. In *Advances in Neural Information Processing Systems*, volume 36.
- Chen, J.; Zhang, Z.; Cao, Z.; Wu, Y.; Ma, Y.; Ye, T.; and Wang, J. 2023b. Neural Multi-Objective Combinatorial Optimization with Diversity Enhancement. In *Advances in Neural Information Processing Systems*, volume 37.
- Choo, E. U.; and Atkins, D. R. 1983. Proper Efficiency in Nonconvex Multicriteria Programming. *Mathematics of Operations Research*, 8(3): 467–470.
- Deb, K.; Pratap, A.; Agarwal, S.; and Meyarivan, T. 2002. A Fast and Elitist Multiobjective Genetic Algorithm: NSGA-II. *IEEE Transactions on Evolutionary Computation*, 6(2): 182–197.
- Drakulic, D.; Michel, S.; and Andreoli, J.-M. 2025. GOAL: A Generalist Combinatorial Optimization Agent Learner. In *International Conference on Learning Representations*, volume 13.
- Drakulic, D.; Michel, S.; Mai, F.; Sors, A.; and Andreoli, J.-M. 2023. BQ-NCO: Bisimulation Quotienting for Efficient Neural Combinatorial Optimization. In *Advances in Neural Information Processing Systems*, volume 37.
- Ehrgott, M. 2005. *Multicriteria Optimization*. Springer Berlin, Heidelberg.
- Ehrgott, M.; and Gandibleux, X. 2000. A survey and Annotated Bibliography of Multiobjective Combinatorial Optimization. *OR-Spektrum*, 22(4): 425–460.
- Fan, M.; Wu, Y.; Cao, Z.; Song, W.; Sartoretti, G.; Liu, H.; and Wu, G. 2025. Conditional Neural Heuristic for Multi-objective Vehicle Routing Problems. *IEEE Transactions on Neural Networks and Learning Systems*, 36(3): 4677–4689.
- Fu, Z.-H.; Qiu, K.-B.; and Zha, H. 2021. Generalize a Small Pre-trained Model to Arbitrarily Large TSP Instances. In *Proceedings of the AAAI Conference on Artificial Intelligence*, volume 35.
- Gaile, E.; Draguns, A.; Ozoliņš, E.; and Freivalds, K. 2022. Unsupervised Training for Neural TSP Solver. In *Learning and Intelligent Optimization*.
- Garaix, T.; Artigues, C.; Feillet, D.; and Josselin, D. 2010. Vehicle Routing Problems with Alternative Paths: An Application to On-Demand Transportation. *European Journal of Operational Research*, 204(1): 62–75.
- Helsgaun, K. 2017. An Extension of the Lin-Kernighan-Helsgaun TSP Solver for Constrained Traveling Salesman and Vehicle Routing Problems. Technical report, Roskilde University.
- Ishibuchi, H.; and Murata, T. 1998. A Multi-Objective Genetic Local Search Algorithm and its Application to Flowshop Scheduling. *IEEE Transactions on Systems, Man, and Cybernetics, Part C*, 28(3): 392–403.
- Jaszkievicz, A. 2002. Genetic local search for multi-objective combinatorial optimization. *European Journal of Operational Research*, 137(1): 50–71.
- Jin, Y.; Ding, Y.; Pan, X.; He, K.; Zhao, L.; Qin, T.; Song, L.; and Bian, J. 2023. Pointerformer: Deep Reinforced Multi-Pointer Transformer for the Traveling Salesman Problem. In *Proceedings of the AAAI Conference on Artificial Intelligence*, volume 37.
- Joshi, C. K.; Laurent, T.; and Bresson, X. 2019. An Efficient Graph Convolutional Network Technique for the Travelling Salesman Problem. ArXiv:1906.01227.
- Kingma, D. P.; and Ba, J. 2015. Adam: A Method for Stochastic Optimization. In *International Conference on Learning Representations*, volume 3.
- Kool, W.; van Hoof, H.; and Welling, M. 2018. Attention, Learn to Solve Routing Problems! In *International Conference on Learning Representations*, volume 7.
- Kwon, Y.-D.; Choo, J.; Kim, B.; Yoon, I.; Gwon, Y.; and Min, S. 2020. POMO: Policy Optimization with Multiple Optima for Reinforcement Learning. In *Advances in Neural Information Processing Systems*, volume 33.
- Kwon, Y.-D.; Choo, J.; Yoon, I.; Park, M.; Park, D.; and Gwon, Y. 2021. Matrix Encoding Networks for Neural Combinatorial Optimization. In *Advances in Neural Information Processing Systems*, volume 34.
- Lacomme, P.; Prins, C.; and Sevaux, M. 2006. A genetic algorithm for a bi-objective capacitated arc routing problem. *Computers and Operations Research*, 33(12): 3473–3493.

- Lai, D. S.; Caliskan Demirag, O.; and Leung, J. M. 2016. A Tabu Search Heuristic for the Heterogeneous Vehicle Routing Problem on a Multigraph. *Transportation Research Part E: Logistics and Transportation Review*, 86: 32–52.
- Legrand, C.; Cattaruzza, D.; Jourdan, L.; and Kessaci, M.-E. 2025. Improving Neighborhood Exploration into MOEA/D Framework to Solve a Bi-Objective Routing Problem. *International Transactions in Operational Research*, 32(1): 117–143.
- Li, K.; Zhang, T.; and Wang, R. 2021. Deep Reinforcement Learning for Multiobjective Optimization. *IEEE Transactions on Cybernetics*, 51(6): 3103–3114.
- Lin, X.; Yang, Z.; and Zhang, Q. 2022. Pareto Set Learning for Neural Multi-Objective Combinatorial Optimization. In *International Conference on Learning Representations*, volume 10.
- Lischka, A.; Wu, J.; Chehreghani, M. H.; and Kulcsár, B. 2024. A GREAT Architecture for Edge-Based Graph Problems Like TSP. arXiv:2408.16717.
- Liu, S.; Chen, J.; and Weiszer, M. 2022. Multi-objective Multigraph A\* Search with Learning Heuristics based on Node Metrics and Graph Embedding. In *IEEE International Conference on Intelligent Systems*, volume 11.
- Lu, Y.; Di, Z.; Li, B.; Liu, S.; Qian, H.; Yang, P.; Tang, K.; and Zhou, A. 2024. Towards Geometry-Aware Pareto Set Learning for Neural Multi-Objective Combinatorial Optimization. ArXiv:2405.08604.
- Maggioni, F.; Perboli, G.; and Tadei, R. 2014. The Multi-path Traveling Salesman Problem with Stochastic Travel Costs: Building Realistic Instances for City Logistics Applications. *Transportation Research Procedia*, 3: 528–536.
- Navon, A.; Shamsian, A.; Chechik, G.; and Fetaya, E. 2021. Learning the Pareto Front with Hypernetworks. In *International Conference on Learning Representations*, volume 9.
- Qiu, R.; Sun, Z.; and Yang, Y. 2022. DIMES: A Differentiable Meta Solver for Combinatorial Optimization Problems. In *Advances in Neural Information Processing Systems*, volume 35.
- Santiyuda, G.; Wardoyo, R.; Pulungan, R.; and Yu, V. F. 2024. Multi-Objective Reinforcement Learning for Bi-Objective Time-Dependent Pickup and Delivery Problem with Late Penalties. *Engineering Applications of Artificial Intelligence*, 128: 107381.
- Sun, Z.; and Yang, Y. 2023. DIFUSCO: Graph-based Diffusion Solvers for Combinatorial Optimization. In *Advances in Neural Information Processing Systems*, volume 37.
- Tadei, R.; Perboli, G.; and Perfetti, F. 2017. The Multi-Path Traveling Salesman Problem with Stochastic Travel Costs. *EURO Journal on Transportation and Logistics*, 6(1): 3–23.
- Tikani, H.; Setak, M.; and Demir, E. 2021. Multi-Objective Periodic Cash Transportation Problem with Path Dissimilarity and Arrival Time Variation. *Expert Systems with Applications*, 164: 114015.
- Vaswani, A.; Shazeer, N.; Parmar, N.; Uszkoreit, J.; Jones, L.; Gomez, A. N.; Kaiser, L. u.; and Polosukhin, I. 2017. Attention is All you Need. In *Advances in Neural Information Processing Systems*, volume 30.
- Vinyals, O.; Fortunato, M.; and Jaitly, N. 2015. Pointer Networks. In *Advances in Neural Information Processing Systems*, volume 28.
- Weiszer, M.; Burke, E. K.; and Chen, J. 2020. Multi-objective Routing and Scheduling for Airport Ground Movement. *Transportation Research Part C: Emerging Technologies*, 119: 102734.
- Wu, H.; Wang, J.; and Zhang, Z. 2020. MODRL/D-AM: Multiobjective Deep Reinforcement Learning Algorithm Using Decomposition and Attention Model for Multi-objective Optimization. In *Artificial Intelligence Algorithms and Applications*.
- Ye, H.; Wang, J.; Liang, H.; Cao, Z.; Li, Y.; and Li, F. 2024. GLOP: Learning Global Partition and Local Construction for Solving Large-scale Routing Problems in Real-time. In *Proceedings of the AAAI Conference on Artificial Intelligence*, volume 38.
- Zhang, Q.; and Li, H. 2007. MOEA/D: A Multiobjective Evolutionary Algorithm Based on Decomposition. *IEEE Transactions on Evolutionary Computation*, 11(6): 712–731.
- Zhang, Z.; Wu, Z.; Zhang, H.; and Wang, J. 2021. Meta-Learning-Based Deep Reinforcement Learning for Multiobjective Optimization Problems. *IEEE Transactions on Neural Networks and Learning Systems*, 34: 7978–7991.
- Zhou, Y.; Kong, L.; and Wang, H. 2025. A Multiobjective Edge-Based Learning Algorithm for the Vehicle Routing Problem with Time Windows. *Information Sciences*, 715: 122223.
- Zitzler, E.; Thiele, L.; Laumanns, M.; Fonseca, C.; and da Fonseca, V. 2003. Performance Assessment of Multi-objective Optimizers: an Analysis and Review. *IEEE Transactions on Evolutionary Computation*, 7(2): 117–132.

## A Architecture Details

Here, we highlight some of the main components in the model architectures that are not described in the main text.

### A.1 Edge-Based Decoder in GMS-EB

In GMS-EB, we utilize an edge-based multi-pointer decoder which is based on Jin et al. (2023). Its mathematical formulation is the following. Given trainable weight matrices  $W_1, W_2, W_3, W_4$  we form the query, representing the current routing context, as

$$q_t = W_1 h_{\pi_1} + W_2 h_{\pi_{t-1}} + \frac{1}{N} (W_3 h_{\text{graph}} + W_4 h_{\text{visited}}).$$

Here,  $h$  denotes an edge-embedding from the encoder,  $\pi_1$  is the first visited edge and  $\pi_{t-1}$  the most recently visited edge. Moreover, we utilize an enhanced context in which  $h_{\text{graph}}$  is the sum of all embeddings in the graph and  $h_{\text{visited}}$  is the sum over the visited edges according to

$$h_{\text{visited}} = \sum_{t'=1}^{t-1} h_{\pi_{t'}}.$$

Let  $H$  be the number of heads/pointers. The score for edge  $l$  is formed according to

$$\alpha_l = \frac{1}{H} \sum_{h=1}^H \frac{1}{\sqrt{d_k}} (W_h^q q_t)^T (W_h^k k_l) - \text{Scalar cost}(l). \quad (6)$$

Note that the key  $k_l$  is the embedding for the edge and  $d_k$  is its dimension. Similarly to the original article, we subtract a cost to speed up the exploration and ensure that costly edges are considered less favorable from the start. In our case, the cost is multi-objective so we must scalarize it. We find that both Chebyshev and linear scalarization work well for this purpose. The last step is to form the logits as

$$u_l = \begin{cases} c \tanh \alpha_l & \text{if } l \text{ connects current and unvisited node} \\ -\infty & \end{cases}$$

Finally, softmax is applied to transform the logits to probabilities.

It must be noted that in our case, we preference-condition the decoder using a hyper-network. This is done by letting a network generate the weights  $W_1, W_2, W_3, W_4$  and  $(W_h^q, W_h^k)_{h=1}^H$ .

### A.2 Selection-Decoder in GMS-DH

The task of this decoder is to prune parallel edges in the intermediate stage of GMS-DH, leaving only one between each node pair. Initially, we apply  $L_3$  GREAT NB layers on the edge embeddings from the encoder to obtain embeddings specialized for this task. In the experiments we set  $L_3 = 2$ . These layers are not preference conditioned. Hence, they do not need to be rerun for each preference. Next, given two nodes, we want to compute the probability of retaining each (directed) edge in between. For this purpose, we essentially utilize a multi-pointer score calculation similar to (6). Given

a node pair  $(i, j)$ , and the set of edges in between,  $E_{ij}$ , let the query be the average embedding according to

$$q_{ij} = \frac{1}{|E_{ij}|} \sum_{l \in E_{ij}} e_l.$$

Moreover, let the key  $k_l$  be the embedding  $e_l$ . Then, form the score for edge  $l$  as

$$\alpha_l = \frac{1}{H} \sum_{h=1}^H \frac{1}{\sqrt{d_k}} (W_h^q q_{ij})^T (W_h^k k_l) - \text{Scalar cost}(l),$$

where  $i = \text{start}(l)$  and  $j = \text{end}(l)$ . Again, note that we subtract a scalar cost to improve exploration. Also note that  $(W_h^q, W_h^k)_{h=1}^H$  are generated by a hyper-network. Final edge probabilities are then computed using tanh-clipping and softmax as

$$u_l = c \tanh(\alpha_l),$$

$$p_l = \frac{\exp(u_l)}{\sum_{l' \in E_{ij}} \exp(u_{l'})}.$$

### A.3 MatNet-Based Benchmark Model

We visualize this architecture in Figure 3. The encoder consists of  $L$  MatNet-layers (Kwon et al. 2021), while the decoder consists of an MP decoder (Jin et al. 2023) preference-conditioned with a hyper-network. The MatNet-architecture operates on bipartite graphs. It utilizes mixed-score attention layers together with fully-connected layers and normalization as in standard transformer layers (Vaswani et al. 2017). These attention layers "mix" internally computed attention scores with external information from e.g. a distance matrix  $D$ . To accommodate the use of several distance matrices,  $D_1, \dots, D_f$  in our multi-objective setting, we follow the idea in Appendix A of the original paper. That is, we mix the internal attention score with all distance matrices using an MLP with  $f + 1$  inputs.

For the node-input to the initial MatNet-layer, in the absence of node-features we use zero-vectors for the "row" nodes and one-hot vectors for the "column" nodes, as in the original paper. If there are node features, e.g., demand in the MOCVRP, we use these as "row" input while keeping the one-hot "column" input. This allows us to augment each instance by sampling several one-hot combinations rather than scaling the instance as is done for GMS.

Lastly, we note that MatNet is not well-defined on multi-graphs due to the fact that it utilizes the distance matrix to represent unique distances between nodes. It is possible to cast multigraphs into simple graphs, but not without increasing the number of nodes and edges drastically. Thus, we must pre-prune a multigraph before passing it through the encoder. This can be done with some sort of heuristic in the general case, but, as discussed, under LS and considering the MOTSP, a simple pruning method is to remove edges with sub-optimal linearly scalarized cost. Moreover, it can be noted that the encoder needs to be rerun for each new preference, which results in a slower architecture than if the encoding is done once.

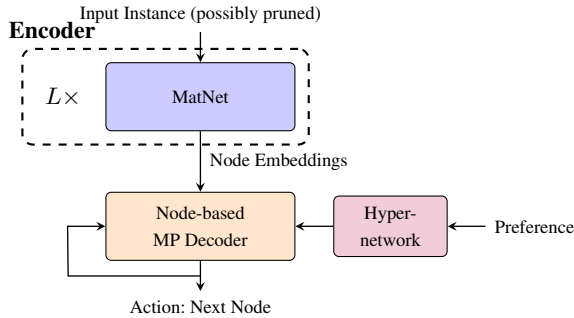


Figure 3: MatNet-Based Model (MBM)

## B Model Training

Here we outline the curriculum learning which we briefly discussed in the main text. We also present an analysis of training performance.

### B.1 Curriculum Learning Details

For both GMS-EB and GMS-DH we utilize a simple curriculum learning approach, with the purpose to decrease training times and to improve performance on large problems. The idea is simple: we train on small instances before training on large instances with the same distribution.

For instances with 20 nodes, we do not use any such curriculum. For instances with 50 nodes we start by training for 100 epochs on 20 nodes and then train on 50 nodes for 100 epochs. Finally, for instances with size 100, we start by training for 100 epochs on size 20. Then, for GMS-DH, we train for 50 epochs on size 50 and 50 epochs on size 100. As GMS-EB takes quite long to train for 100 nodes, we are satisfied with training for 100 epochs on size 50 for this model and then fine-tune it for 10 epochs on size 100, resulting in 210 epochs in total. Remark that our curriculum is quite arbitrary, but the model performance is not contingent on this exact setup.

Additionally, we start by training GMS-DH for 5 epochs (included in the first 100 epochs) on the XASY distribution with 20 nodes. This is because the selection-decoder relies on a reward signal from the routing-decoder. As such, we find that performance and rate of convergence improves if the routing-decoder is pre-trained to obtain a stable and accurate signal. We also find that stability increases if we freeze the parameters of the shared encoder with respect to the loss of the selection-decoder. That is, only the loss from the routing-decoder is utilized to calculate encoder gradients.

### B.2 Training Times

Table 5 shows the number of parameters for the models as well as training time per epoch for one problem on a Simple Graph (SG) and Multigraph (MG). The SG problem is the MOTSP with 50 nodes, while the MG problem is the MG-MOTSP with 50 nodes and 2 parallel edges. It can be noted that GMS-EB takes a very long time to train, especially on multigraphs, while GMS-DH is more efficient and MBM is

	#Params Enc.	#Params Dec.	Epoch SG	Epoch MG
MBM	2.38M	266K	4.7m	4.7m
GMS-DH	2.06M	1.08M	8.4m	24m
GMS-EB	1.98M	266K	51m	1.7h

Table 5: Number of parameters and time per epoch for the models. For GMS-DH, the parameters in the decoder refers to both decoders.

the most efficient. In fact, MBM is not affected by the multi-graph representation as it works on pruned graphs.

We want to highlight that the training performance is a weakness of GMS. However, these models are very sample efficient, which is illustrated on examples with 20 nodes (that is, without curriculum learning) in Figure 4. Moreover, we try to remedy this weakness through the curriculum approach. When utilizing the curriculum learning, it is often enough to train on the small instance sizes to obtain a majority of performance and the rest is obtained after a few epochs of training on the larger instance. This can be seen in Figure 5, which showcases two examples with 50 nodes.

## C Routing Problems and Distributions

In this section, we detail the distributions and routing problems which we solve.

### C.1 Distributions

The following distributions for node distances are used across the problems on simple graphs.

- **EUC** - Euclidean. Here, we sample node coordinates uniformly and independently in the unit square. These are utilized to construct a distance matrix using the Euclidean distance. For a problem with  $m$  node distances (e.g., the MOTSP with  $m$  objectives) we sample  $m$  pairs of coordinates independently.
- **TMAT** - Asymmetric distance matrix obeying the triangle inequality (Kwon et al. 2021). The distance matrix is first populated with random independent elements and then post-processed until the triangle inequality is satisfied. For a problem with  $m$  distances, we sample  $m$  matrices independently.
- **XASY** - Extremely asymmetric distance matrix (Gaile et al. 2022). The distance matrix does not satisfy the triangle inequality. It is obtained by independently sampling each element uniformly between 0 and 1. Again, we sample all  $m$  matrices independently.

The following distributions are used for problems on multigraphs.

- **FLEX $x$**  - Flexible number of edges between each node pair. Here we sample  $x$  vectors of dimension  $m$  representing edge attributes for edges between a node pair. Each attribute for each edge is sampled uniformly between 0 and 1. Then we remove dominated edges until only a Pareto set of edges remains.
- **FIX $x$**  - Fixed number of edges between each node pair. We start by sampling  $x$  vectors in the same way as the

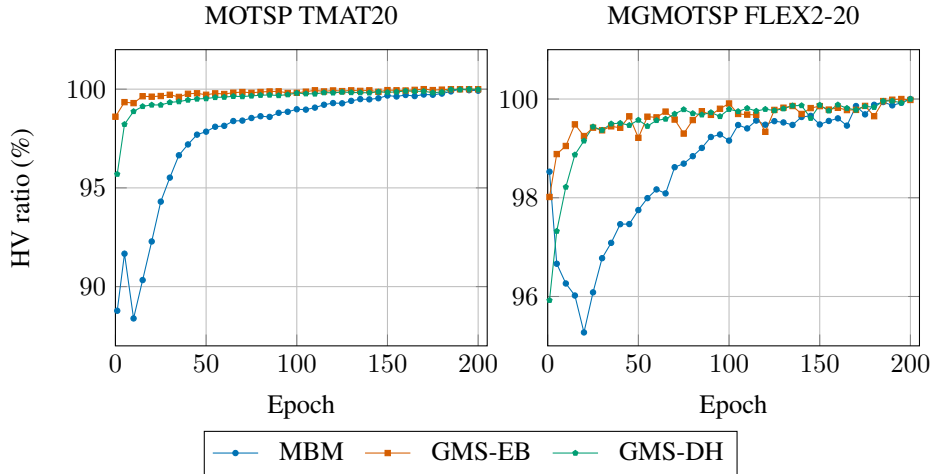


Figure 4: HV as percentage of best performance for models during training. GMS-EB and GMS-DH reach close to their final performance quickly and are more sample-efficient than MBM.

FLEX-distribution. Then we sort each attribute so that no edge is dominated. For  $m = 2$ , we sort one attribute in descending order and one attribute in ascending order.

Note that neither FLEX $x$  nor FIX $x$  obeys the triangle inequality, although such an assumption holds for real instances. We highlight that these distributions are utilized since they are simple and easy to sample from, creating a more transparent picture of the model performance. Motivated by the fact that XASY seems more difficult to learn than TMAT, we hypothesize that the triangle inequality would contribute positively to model performance.

## C.2 MOTSP

**Problem Description:** In the multi-objective traveling salesman problem the goal is to visit all nodes/customers and return to the starting position. The Euclidean version of this problem is widely treated in the learning-for-routing community, see e.g., Lin, Yang, and Zhang (2022) and Fan et al. (2025) in the multi-objective case. In our case, we sample two distances, corresponding to the two objectives, between each pair of customers. The goal is to design a tour that minimizes the sum of the distances. A tour can start from any node.

**Data Generation:** Edge distances are sampled according to the EUC, TMAT and XASY distributions above.

**Model Details:** There are no node features for this problem, hence both the GREAT-based and MatNet-based encoders have the two distances as edge features, while the latter uses zero-vectors as "row" input.

**Evaluation Details:** For all distributions, we utilize (15, 15), (30, 30) and (60, 60) as reference for HV calculation for 20, 50 and 100 nodes respectively. In the zero-shot experiments, we have (90, 90) as reference for 150 nodes and (120, 120) for 200 nodes.

## C.3 MOCVRP

**Problem Description:** In the multi-objective capacitated vehicle routing problem, a truck starts at a depot and must pick up goods from a specified number of customers. The vehicle has a fixed capacity while each customer has a demand. When the capacity is full, the vehicle must return to the depot. As many vehicles as required can be utilized to meet the demand of all customers.

Similarly to the TSP, this problem has been widely treated in the Euclidean setting using learning-based methods. As is common in the multi-objective setting (Lin, Yang, and Zhang 2022), we assume one objective is the traveled distance, while the other is the longest tour for a single vehicle (makespan). As such, each node-pair is only associated with one distance.

**Data Generation:** We assume that the capacity of the truck is 30, 40 and 50 for 20, 50 and 100 nodes respectively, while the demands are sampled uniformly from the set  $\{1, \dots, 9\}$ . This is the same setting as in e.g., Kool, van Hoof, and Welling (2018) and Lin, Yang, and Zhang (2022). Edge distances are sampled according to the EUC, TMAT and XASY distributions.

**Model Details:** In the decoding, we augment the routing context (represented by the query  $q_t$ ) with the current load of the vehicle. For the GREAT-based encoders, we let the features of an edge be its distance as well as the demand of the customer at the end. On the other hand, the MatNet-based encoders only utilize the distance as an edge-feature while the demand is used as a node feature.

**Evaluation Details:** For all distributions, we utilize (15, 3), (40, 3) and (60, 3) as reference for HV calculation for the three considered instance sizes.

## C.4 MGMOTSP

**Problem Description:** As for the MOTSP, the goal of the multigraph MOTSP is to visit all nodes and return to the start. The only difference is that the underlying structure is

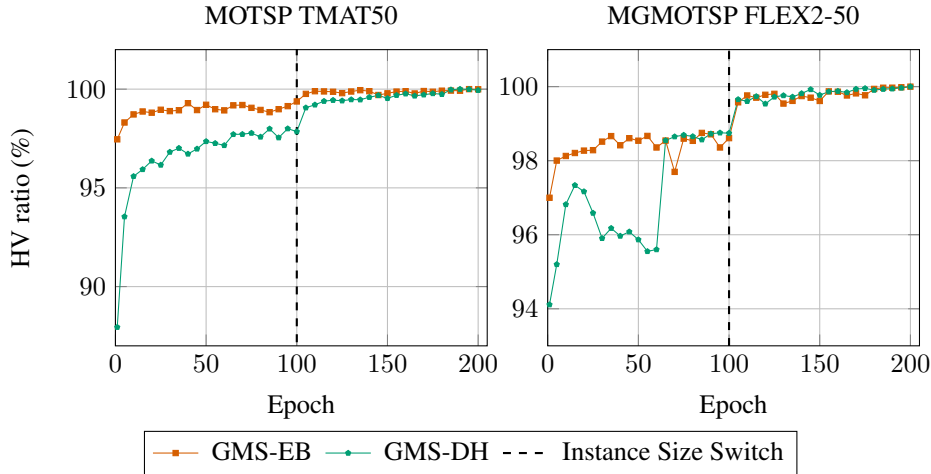


Figure 5: HV as percentage of best performance for GMS during training. It is enough to train on 20 nodes to obtain a majority ( $\approx 98\%$ ) of the performance. After 5 epochs of training on instances with 50 nodes, the models reach  $> 99.5\%$  of their final performance.

a multigraph. Similarly, we define two distances for each node pair and these are associated with the objectives of the problem.

While this variant of the TSP on a multigraph has not been treated before to our knowledge (neither using learning nor other methods), some stochastic single-objective variants have been proposed in e.g., Tadei, Perboli, and Perfetti (2017) and Maffioli, Perboli, and Tadei (2014). Moreover, we believe that the MG MOTSP is a suitable benchmark problem for our solvers, as it is simple and easy to find good baselines for.

**Data Generation:** We sample distances between the nodes according to the  $FLEX_x$  and  $FIX_x$  distributions.

**Model Details:** As the MOTSP, the MG MOTSP lacks edge features. Hence, we utilize the same setup for the models as in the MOTSP. Moreover, for the MatNet-based model, we sparsify the underlying multigraph given each preference before it is fed into the encoder. This is done by removing all edges with sub-optimal LS cost compared to a parallel edge. To make this pruning strategy exact, we train MBM using linearly scalarized reward instead of the Chebyshev reward.

**Evaluation Details:** For the  $FLEX_x$  distribution, we utilize  $(15, 15)$ ,  $(30, 30)$  and  $(60, 60)$  as reference for instance sizes 20, 50 and 100, regardless of  $x$ . In the zero-shot experiments we set the references to  $(90, 90)$  and  $(120, 120)$  for  $FLEX_x$  with 150 and 200 nodes. For  $FIX_x$ , the reference is given by  $(N, N)$ , where  $N$  is the node count.

## C.5 MG MOTSP TW

**Problem Description:** The goal in MG MOTSP TW is to create a tour that visits all customers and returns to the starting position. However, in this case we assume there is a fixed depot and that each customer/node is associated with a time-window. Preferably, the vehicle should arrive within the time-window for each customer. As such, we let one ob-

jective be the number of violated time-windows while the other is the traveled distance. Accordingly, each edge connecting two locations is associated with a travel time and a distance.

Multi-objective problems with similar objectives are fairly widespread in literature (Legrand et al. 2025), although not on multigraphs. In the multigraph framework, this problem is reminiscent of the vehicle routing problem with time-windows in Ben Ticha et al. (2017), but with a second objective that is the soft variant of the time-window constraint.

**Data Generation:** Distances and travel times are sampled according to the  $FLEX_x$  and  $FIX_x$  distributions. Additionally, we sample time-windows according to the "medium" distribution of Chen et al. (2024) and Bi et al. (2024). In this setting, time-windows are sampled uniformly and independently, which results in difficult instances where there is a true trade-off between optimal paths and paths satisfying the time-window constraint. We also argue that this premise is simple for initial evaluation of our models, especially in comparison to e.g., the "hard" instances of Chen et al. (2024), which tests out-of-distribution generalization.

Further, we assume that the vehicle can depart immediately from each customer, i.e., that there is no service time, and that no waiting occurs, even if a vehicle arrives before the starting time. The latter is for simplicity, as in general how long the vehicle should wait at a node is a decision in itself. We also argue that this assumption is fairly realistic.

**Model Details:** In the decoder, we enhance the routing context with an embedding of the current time. In the encoder, the node features in this case are the starting time and end time of the service, while the edge features are distance and travel time. Consequently, we augment the input features of GREAT so that an edge is associated with its distance, travel time and the time-window of the ending node. As usual for MatNet, the node features are used as "row" in-

puts while the edge features are used in the distance matrix.

Note that in this case, pruning of the multigraph for MatNet is not obvious. For instance, removing an edge with a high travel time but low distance might not be optimal if traversing that edge would result in no violated time-windows anyway. Consequently, we apply the same simple pruning method as for the MGMOTSP. That is, we form the cost of each edge using a linear combination of its travel time and distance, then we remove all edges apart from the best one. We also choose the linear reward instead of the Chebyshev reward for MBM.

**Evaluation Details:** In this case, we let the reference value corresponding to the time-window violation be  $N + 5$ , while the reference value corresponding to the distance is the same as in the MGMOTSP case.

## D Setup for MOEAS

As a base for the implementation of NSGA-II, NSGA-III and MOEA/D, we utilized Pymoo<sup>2</sup> and as a base for MOGLS, we utilized GeneticLocalSearch\_TSP<sup>3</sup>. For the former three, we limit the number of iterations to 1000 while the latter is limited to 10000. Additionally, local search strategies is a necessity for efficient usage of genetic algorithms in combinatorial optimization. For the MOTSP, we utilized the 2-opt heuristic of Jaszkiwicz (2002), while we utilized the problem-specific local search and chromosome decoding strategy of Lacomme, Prins, and Sevaux (2006) for the MOCVRP.

However, in both cases we find that by accepting the best local move instead of just an improving one, the performance on large asymmetric problems improves substantially. As this affects the runtime negatively (due to the need to search through all moves), we limit the number of local moves in each search depending on the problem size. Additionally, for the algorithms not requiring preference weights for each individual, we must calculate such weights to compare the improvements. In the bi-objective case, this is done using the strategy of Lacomme, Prins, and Sevaux (2006) according to

$$\begin{aligned}\tilde{w}_1(S) &= (f_1(S) - f_1^{\min}) / (f_1^{\max} - f_1^{\min}), \\ \tilde{w}_2(S) &= (f_2(S) - f_2^{\min}) / (f_2^{\max} - f_2^{\min}), \\ w_1(S) &= \tilde{w}_1(S) / (\tilde{w}_1(S) + \tilde{w}_2(S)), \\ w_2(S) &= \tilde{w}_2(S) / (\tilde{w}_1(S) + \tilde{w}_2(S)),\end{aligned}$$

where  $S$  is the solution being evaluated and  $f_i^{\min}, f_i^{\max}, i = 1, 2$  are minimum and maximum values for the respective objectives.

In the multigraph setting, we design our own setup to tailor the MOEAS. To start with, inspired by one representation from Beke, Weiszner, and Chen (2021) regarding shortest path problems, we let a chromosome for a tour be given by a permutation of the nodes multiplied with 100 added with the index of the edge to the next node. For example, in an MGMOTSP with 2 parallel edges and 5 nodes, a chromosome

might be

$$(101, 302, 201, 501, 402).$$

For the mutation operator, we randomly either change one edge or reverse a segment of the tour. For the crossover, we utilize an edge recombination operator. Regarding the local search, we use a variant of 2-opt where we again accept the best local move. A local move is defined by a standard 2-opt move with the nodes, together with new edge selections given the changed node order. This edge selection is found by choosing the edge with the lowest LS cost between nodes that were previously not neighbors or have changed order.

We want to stress that the focus in this study is not to design an evolutionary algorithms, we simply want a baseline to compare against. We find that the proposed approach is somewhat efficient for small node counts, but performs quite badly for large graphs.

## E Complementary Numerical Results

In this section, we show additional numerical results for more distributions, benchmarks and instance sizes.

### E.1 Problems on Simple Graphs

Table 6 and 7 show results for the MOTSP and MOCVRP respectively. Apart from the benchmarks in the main text, we present the performance of three simple heuristics: Nearest Neighbor (NN), Nearest Insertion (NI) and Farthest Insertion (FI). As LKH and OR-tools, these utilize the linear scalarization to transform the MO problem into single-objective subproblems. Additionally, we show results on Euclidean instances (EUC). For these, there are many existing models in literature and thus we replace MBM with the Conditional Neural Heuristic (CNH) of Fan et al. (2025). This model is augmented with the Euclidean augmentation of Lin, Yang, and Zhang (2022).

On the EUC distribution, our models are generally slightly worse than CNH. This is to be expected though, as a common pattern in previous studies is that architectures built for directed graph inputs perform worse on EUC than those specialized for coordinate inputs (Lischka et al. 2024; Kwon et al. 2021).

### E.2 Multigraph Problems

We display additional results for the MGMOTSP and MGMOTSPTW in Tables 8-10. As for the MOTSP, we include NN, NI and FI for MGMOTSP. In the case of MGMOTSPTW, we also include results for LKH and OR-tools when treating the problem as the MGMOTSP. That is, we neglect the time-windows and treat the time duration of each edge exactly as the distance. We call these methods implicit LKH and implicit OR-tools, as they implicitly minimize the time-window violations by reducing the time the tour takes.

### E.3 Generalization to Larger Instances

In Tables 11-12, we report the generalization performance zero-shot for our methods in the MOTSP and MGMOTSP cases. It can be seen that both models retain competitive performance. In particular, GMS-EB often performs close to LKH while being faster.

<sup>2</sup><https://pymoo.org/>

<sup>3</sup>[https://github.com/kevin031060/Genetic\\_Local\\_Search\\_TSP](https://github.com/kevin031060/Genetic_Local_Search_TSP)

	EUC20			EUC50			EUC100		
	HV	Gap	Time	HV	Gap	Time	HV	Gap	Time
LKH	0.52	0.00%	(2.6m)	0.58	0.00%	(14m)	0.68	0.00%	(1.2h)
OR Tools	0.51	0.97%	(2.0m)	0.57	1.83%	(15m)	0.67	1.57%	(1.3h)
NN	0.46	11.44%	(1.9s)	0.51	11.42%	(7.1s)	0.63	8.23%	(25s)
NI	0.47	8.53%	(11s)	0.52	9.97%	(1.8m)	0.63	7.82%	(12m)
FI	0.50	3.44%	(13s)	0.55	5.79%	(2.1m)	0.65	4.96%	(14m)
MOGLS	<b>0.51</b>	<b>0.79%</b>	(1.0h)	<b>0.58</b>	<b>0.74%</b>	(3.8h)	<b>0.68</b>	<b>1.16%</b>	(32h)
NSGA-II	0.50	2.63%	(44m)	0.52	11.18%	(3.4h)	0.54	21.13%	(12h)
NSGA-III	0.50	3.56%	(46m)	0.50	14.07%	(3.4h)	0.53	21.82%	(12h)
MOEA/D	0.51	0.87%	(56h)	0.57	2.53%	(3.6h)	0.63	8.08%	(13h)
CNH	0.51	1.16%	(6.5s)	0.57	1.84%	(7.1s)	0.67	1.89%	(25s)
CNH (aug)	0.51	0.85%	(17s)	0.57	1.26%	(44s)	0.67	1.45%	(3.1m)
GMS-EB	0.51	0.93%	(2.0s)	0.57	1.98%	(25s)	0.67	2.34%	(3.6m)
GMS-DH	0.51	1.30%	(1.1s)	0.57	2.64%	(3.8s)	0.67	2.49%	(20s)
GMS-EB (aug)	0.51	0.81%	(14s)	0.57	1.57%	(3.3m)	0.67	2.09%	(28m)
GMS-DH (aug)	0.51	0.93%	(5.3s)	0.57	1.91%	(27s)	0.67	2.24%	(2.6m)
	TMAT20			TMAT50			TMAT100		
LKH	0.58	0.00%	(2.3m)	0.58	0.00%	(6.4m)	0.63	0.00%	(29m)
OR Tools	0.56	3.01%	(3.3m)	0.54	6.13%	(29m)	0.59	7.12%	(2.5h)
NN	0.48	16.66%	(1.9s)	0.47	18.34%	(7.0s)	0.54	15.25%	(25s)
NI	0.53	8.78%	(11s)	0.50	13.17%	(1.8m)	0.55	13.24%	(12m)
FI	0.54	6.60%	(13s)	0.52	10.65%	(2.0m)	0.57	10.84%	(14m)
MOGLS	0.54	7.72%	(20m)	0.40	30.90%	(2.7h)	0.38	40.03%	(19h)
NSGA-II	0.57	2.17%	(44m)	0.51	12.91%	(3.5h)	0.47	25.98%	(12h)
NSGA-III	0.57	2.87%	(45m)	0.50	14.54%	(3.5h)	0.46	27.53%	(13h)
MOEA/D	0.57	1.43%	(56m)	0.53	9.51%	(3.7h)	0.50	20.93%	(13h)
MBM	0.57	2.29%	(1.3s)	0.50	13.51%	(3.9s)	0.56	11.16%	(19s)
MBM (aug)	0.58	0.96%	(5.6s)	0.52	10.17%	(27s)	0.58	9.17%	(2.4m)
GMS-EB	0.58	0.88%	(2.2s)	0.57	1.50%	(25s)	0.63	1.45%	(3.6m)
GMS-DH	0.58	1.08%	(1.3s)	0.57	2.36%	(4.1s)	0.62	2.76%	(20s)
GMS-EB (aug)	<b>0.58</b>	<b>0.67%</b>	(15s)	<b>0.57</b>	<b>1.14%</b>	(3.3m)	<b>0.63</b>	<b>1.13%</b>	(29m)
GMS-DH (aug)	0.58	0.79%	(5.6s)	0.57	1.76%	(28s)	0.62	2.19%	(2.6m)
	XASY20			XASY50			XASY100		
LKH	0.75	0.00%	(2.3m)	0.83	0.00%	(6.9m)	0.90	0.00%	(32m)
OR Tools	0.71	5.49%	(3.0m)	0.77	7.25%	(24m)	0.85	6.06%	(1.8h)
NN	0.60	20.11%	(1.8s)	0.70	16.32%	(7.0s)	0.80	10.94%	(25s)
NI	0.61	17.76%	(11s)	0.66	21.37%	(1.8m)	0.73	18.88%	(12m)
FI	0.60	19.57%	(12s)	0.64	23.62%	(2.1m)	0.72	20.42%	(14m)
MOGLS	0.65	13.23%	(19m)	0.51	39.16%	(2.6h)	0.47	47.82%	(19h)
NSGA-II	0.72	4.06%	(44m)	0.70	15.63%	(3.5h)	0.64	29.74%	(13h)
NSGA-III	0.71	4.56%	(45m)	0.70	16.64%	(3.5h)	0.63	30.13%	(13h)
MOEA/D	0.73	2.68%	(56m)	0.73	12.68%	(3.6h)	0.70	22.22%	(13h)
MBM	0.68	9.10%	(1.4s)	0.75	10.37%	(3.7s)	0.84	7.41%	(19s)
MBM (aug)	0.70	5.86%	(5.5s)	0.76	8.28%	(27s)	0.85	6.34%	(2.4m)
GMS-EB	0.73	1.95%	(2.3s)	0.81	2.94%	(25s)	0.88	3.03%	(3.6m)
GMS-DH	0.73	2.37%	(1.9s)	0.80	4.12%	(3.9s)	0.86	4.87%	(20s)
GMS-EB (aug)	<b>0.74</b>	<b>1.30%</b>	(15s)	<b>0.82</b>	<b>2.06%</b>	(3.3m)	<b>0.88</b>	<b>2.76%</b>	(28m)
GMS-DH (aug)	0.74	1.57%	(5.8s)	0.81	2.84%	(28s)	0.87	3.85%	(2.6m)

Table 6: MOTSP with different instance sizes (20, 50 and 100) and distributions.

	EUC20			EUC50			EUC100		
	HV	Gap	Time	HV	Gap	Time	HV	Gap	Time
MOGLS	0.23	3.35%	(4.1h)	0.17	37.39%	(26h)	0.00	100.00%	(108h)
NSGA-II	0.23	0.13%	(2.6h)	0.27	2.14%	(24h)	0.20	18.91%	(75h)
NSGA-III	0.23	0.21%	(2.7h)	0.26	2.91%	(25h)	0.20	21.23%	(75h)
MOEA/D	0.23	0.90%	(2.9h)	0.26	2.73%	(25h)	0.23	7.40%	(73h)
CNH	0.23	0.77%	(5.0s)	0.27	0.59%	(9.5s)	0.25	0.56%	(29s)
CNH (aug)	<b>0.23</b>	<b>0.00%</b>	(29s)	<b>0.27</b>	<b>0.00%</b>	(58s)	<b>0.25</b>	<b>0.00%</b>	(3.6m)
GMS-EB	0.23	0.30%	(3.4s)	0.27	0.44%	(33s)	0.25	0.56%	(4.1m)
GMS-DH	0.23	1.33%	(2.3s)	0.27	1.11%	(6.6s)	0.25	1.36%	(30s)
GMS-EB (aug)	0.23	0.13%	(22s)	0.27	0.18%	(4.7m)	0.25	0.32%	(54m)
GMS-DH (aug)	0.23	0.90%	(10s)	0.27	0.66%	(46s)	0.25	0.92%	(4.1m)
	TMAT20			TMAT50			TMAT100		
MOGLS	0.40	1.78%	(4.1h)	0.31	35.06%	(28h)	0.05	89.38%	(116h)
NSGA-II	0.40	1.38%	(2.7h)	0.36	23.04%	(23h)	0.13	71.72%	(76h)
NSGA-III	0.40	1.98%	(2.7h)	0.35	25.91%	(24h)	0.12	74.11%	(76h)
MOEA/D	0.39	2.59%	(3.0h)	0.41	13.98%	(24h)	0.19	58.70%	(76h)
MBM	0.40	1.14%	(2.4s)	0.47	1.33%	(6.2s)	0.43	4.50%	(27s)
MBM (aug)	0.40	0.86%	(10s)	0.47	0.99%	(41s)	0.44	3.29%	(3.3m)
GMS-EB	0.40	0.25%	(3.5s)	0.47	0.25%	(36s)	0.45	0.57%	(4.2m)
GMS-DH	0.40	0.64%	(2.5s)	0.47	0.76%	(6.8s)	0.45	1.46%	(32s)
GMS-EB (aug)	<b>0.41</b>	<b>0.00%</b>	(23s)	<b>0.47</b>	<b>0.00%</b>	(5.2m)	<b>0.45</b>	<b>0.00%</b>	(33m)
GMS-DH (aug)	0.40	0.32%	(10s)	0.47	0.36%	(47s)	0.45	0.79%	(4.3m)
	XASY20			XASY50			XASY100		
MOGLS	0.59	2.39%	(4.0h)	0.49	34.85%	(29h)	0.13	83.50%	(121h)
NSGA-II	0.60	1.24%	(2.7h)	0.55	27.19%	(24h)	0.28	64.39%	(85h)
NSGA-III	0.59	2.21%	(2.7h)	0.52	31.06%	(25h)	0.25	68.40%	(86h)
MOEA/D	0.59	3.24%	(3.0h)	0.65	13.88%	(24h)	0.42	47.23%	(83h)
MBM	0.57	5.95%	(2.3s)	0.70	6.57%	(6.2s)	0.60	24.47%	(27s)
MBM (aug)	0.59	3.06%	(10s)	0.72	4.13%	(42s)	0.64	19.60%	(3.4m)
GMS-EB	0.60	1.44%	(3.5s)	0.74	1.89%	(36s)	0.79	1.23%	(4.3m)
GMS-DH	0.58	3.40%	(2.4s)	0.72	4.13%	(6.6s)	0.77	3.60%	(33s)
GMS-EB (aug)	<b>0.61</b>	<b>0.00%</b>	(23s)	<b>0.75</b>	<b>0.00%</b>	(5.0m)	<b>0.80</b>	<b>0.00%</b>	(48m)
GMS-DH (aug)	0.60	1.29%	(10s)	0.74	1.65%	(47s)	0.79	1.21%	(4.7m)

Table 7: MOCVRP with different instance sizes (20, 50 and 100) and distributions.

	FLEX2-20			FLEX2-50			FLEX2-100		
	HV	Gap	Time	HV	Gap	Time	HV	Gap	Time
LKH	0.85	0.00%	(1.2m)	0.90	0.00%	(6.3m)	0.94	0.00%	(31m)
OR Tools	0.82	3.30%	(3.0m)	0.86	4.21%	(24m)	0.91	3.46%	(1.8h)
NN	0.74	13.34%	(1.9s)	0.81	10.38%	(7.1s)	0.88	6.71%	(25s)
NI	0.75	11.13%	(9.6s)	0.78	13.13%	(1.7m)	0.84	11.32%	(12m)
FI	0.75	11.98%	(12s)	0.77	14.30%	(2.0m)	0.83	12.20%	(14m)
MOGLS	0.71	16.29%	(1.9h)	0.49	45.84%	(29h)	0.43	54.91%	(18h)
NSGA-II	0.81	5.06%	(1.3h)	0.74	17.62%	(19h)	0.64	32.11%	(15h)
NSGA-III	0.80	5.82%	(1.3h)	0.74	18.48%	(19h)	0.63	33.16%	(14h)
MOEA/D	0.80	6.02%	(1.4h)	0.74	17.50%	(18h)	0.66	30.28%	(12h)
MBM	0.82	3.30%	(4.4s)	0.86	5.21%	(13s)	0.91	3.72%	(44s)
MBM (aug)	0.84	1.50%	(32s)	0.87	3.98%	(1.7m)	0.91	3.28%	(5.9m)
GMS-EB	0.83	1.61%	(4.0s)	0.88	2.00%	(56s)	0.93	1.81%	(9.1m)
GMS-DH	0.84	1.34%	(3.2s)	0.89	1.84%	(13s)	0.92	2.11%	(49s)
GMS-EB (aug)	0.84	0.95%	(34s)	0.89	1.50%	(7.5m)	<b>0.93</b>	<b>1.47%</b>	(1.2h)
GMS-DH (aug)	<b>0.84</b>	<b>0.86%</b>	(19s)	<b>0.89</b>	<b>1.45%</b>	(1.5m)	0.93	1.61%	(6.6m)

Table 8: MGMOTSP on FLEX $x$  with different instances sizes (20, 50 and 100).

	FIX2-20			FIX2-50			FIX2-100		
	HV	Gap	Time	HV	Gap	Time	HV	Gap	Time
LKH	0.85	0.00%	(1.2m)	0.92	0.00%	(6.3m)	0.95	0.00%	(30m)
OR Tools	0.83	2.42%	(2.9m)	0.90	2.59%	(24m)	0.93	2.25%	(2.0h)
NN	0.77	9.86%	(1.9s)	0.86	6.34%	(7.1s)	0.91	4.23%	(25s)
NI	0.78	8.39%	(9.6s)	0.85	7.95%	(1.7m)	0.88	7.14%	(12m)
FI	0.78	9.23%	(11s)	0.84	8.82%	(2.0m)	0.88	7.89%	(14m)
MOGLS	0.74	13.68%	(1.9h)	0.65	29.64%	(29h)	0.52	45.00%	(19h)
NSGA-II	0.81	5.64%	(1.3h)	0.77	16.56%	(19h)	0.69	27.94%	(15h)
NSGA-III	0.80	6.85%	(1.3h)	0.75	18.79%	(19h)	0.66	30.49%	(15h)
MOEA/D	0.80	6.20%	(1.4h)	0.78	15.42%	(18h)	0.69	27.63%	(12h)
MBM	0.84	1.57%	(4.4s)	0.90	2.46%	(13s)	0.93	2.41%	(44s)
MBM (aug)	<b>0.85</b>	<b>0.50%</b>	(32s)	0.91	1.66%	(1.7m)	0.93	2.10%	(5.9m)
GMS-EB	0.84	1.46%	(3.9s)	0.91	1.27%	(57s)	0.94	1.33%	(9.2m)
GMS-DH	0.84	1.37%	(3.2s)	0.91	1.73%	(12s)	0.93	2.13%	(52s)
GMS-EB (aug)	0.85	0.99%	(28s)	<b>0.91</b>	<b>1.02%</b>	(7.5m)	<b>0.94</b>	<b>1.09%</b>	(1.2h)
GMS-DH (aug)	0.85	0.82%	(18s)	0.91	1.40%	(1.5m)	0.93	1.92%	(6.6m)

Table 9: MGMOTSP on FIX $x$  with different instances sizes (20, 50 and 100).

	FLEX2-20			FLEX2-50		
	HV	Gap	Time	HV	Gap	Time
Implicit LKH	0.27	66.74%	(1.1m)	0.14	84.11%	(6.7m)
Implicit OR Tools	0.24	70.78%	(3.4m)	0.13	85.34%	(25m)
MOGLS	0.64	22.92%	(2.7h)	0.35	60.96%	(21h)
NSGA-II	0.69	16.55%	(2.4h)	0.51	43.47%	(35h)
NSGA-III	0.69	16.01%	(2.5h)	0.50	44.53%	(36h)
MOEA/D	0.75	9.19%	(2.7h)	0.60	32.79%	(34h)
MBM	0.72	12.89%	(4.9s)	0.80	11.09%	(14s)
MBM (aug)	0.73	11.98%	(34s)	0.81	10.10%	(1.8m)
GMS-EB	0.81	1.95%	(4.3s)	0.89	0.97%	(60s)
GMS-DH	0.80	3.37%	(3.1s)	0.85	5.10%	(13s)
GMS-EB (aug)	<b>0.82</b>	<b>0.00%</b>	(31s)	<b>0.90</b>	<b>0.00%</b>	(7.9m)
GMS-DH (aug)	0.82	0.33%	(16s)	0.87	2.69%	(1.6m)

Table 10: MGMOTSPTW on FLEX $x$  with different instances sizes (20, 50).

	EUC150			EUC200		
	HV	Gap	Time	HV	Gap	Time
LKH	0.73	0.00%	(1.6h)	0.76	0.00%	(3.0h)
OR Tools	<b>0.72</b>	<b>1.38%</b>	(1.7h)	<b>0.75</b>	<b>1.24%</b>	(3.5h)
CNH ZS	0.72	2.04%	(50s)	0.74	2.22%	(1.3m)
GMS-EB ZS	0.71	2.71%	(6.7m)	0.74	2.93%	(17m)
GMS-DH ZS	0.71	2.82%	(30s)	0.74	3.12%	(1.0m)
	TMAT150			TMAT200		
LKH	0.65	0.00%	(39m)	0.67	0.00%	(1.2h)
OR Tools	0.60	7.57%	(3.3h)	0.62	7.89%	(6.5h)
GMS-EB ZS	<b>0.64</b>	<b>1.64%</b>	(6.7m)	<b>0.66</b>	<b>1.86%</b>	(17m)
GMS-DH ZS	0.63	3.20%	(30s)	0.65	3.59%	(1.0m)
	XASY150			XASY200		
LKH	0.93	0.00%	(40m)	0.95	0.00%	(1.3h)
OR Tools	0.88	5.12%	(2.2h)	0.90	4.46%	(4.0h)
GMS-EB ZS	<b>0.90</b>	<b>2.77%</b>	(6.7m)	<b>0.92</b>	<b>2.78%</b>	(17m)
GMS-DH ZS	0.88	5.10%	(30s)	0.90	5.22%	(1.0m)

Table 11: MOTSP for instances with more nodes.

	FLEX2-150			FLEX2-200		
	HV	Gap	Time	HV	Gap	Time
LKH	0.96	0.00%	(39m)	0.97	0.00%	(1.2h)
OR Tools	0.93	2.93%	(2.1h)	0.94	2.53%	(3.9h)
GMS-EB ZS	<b>0.94</b>	<b>1.78%</b>	(18m)	<b>0.95</b>	<b>1.74%</b>	(50m)
GMS-DH ZS	0.94	2.17%	(1.0m)	0.95	2.27%	(2.2m)
	FIX2-150			FIX2-200		
LKH	0.96	0.00%	(39m)	0.97	0.00%	(1.2h)
OR Tools	0.94	1.96%	(2.2h)	0.95	1.73%	(4.0h)
GMS-EB ZS	<b>0.95</b>	<b>1.35%</b>	(18m)	<b>0.96</b>	<b>1.34%</b>	(50m)
GMS-DH ZS	0.94	2.38%	(1.1m)	0.94	2.56%	(2.2m)

Table 12: MGMOTSP for instances with more nodes.